RSC Advances

PAPER

View Article Online
View Journal | View Issue

Cite this: *RSC Adv.*, 2025, **15**, 7649

Open-aired synthesis of star-shaped poly[2-(methacryloyloxy)ethyl trimethylammonium chloride]†

Tomasz Fronczyk,[a] Anna Mielańczyk,*[a] Olesya Klymenko[b] and Dorota Neugebauer[a]

Received 28th January 2025
Accepted 3rd March 2025

DOI: 10.1039/d5ra00674k

rsc.li/rsc-advances

A series of star-shaped poly[2-(methacryloyloxy)ethyl trimethylammonium chloride]s with different arm lengths were synthesized *via* open-aired enzymatically assisted ATRP using the 2-hydroxypropyl β-cyclodextrin derivative as an initiator. The resulting PMETAs with narrow molecular weight distribution ($Đ$ = 1.06–1.12) created thin hydrophilic films with thickness < 40 nm exhibiting water contact angle (WCA) values < 50°. Higher interfacial tension values obtained for star-shaped polymers in comparison with the linear analog indicate that surface wettability can be modified by changing the polymer topology. AFM was used to analyze the relationship between macromolecule topology, surface roughness, and WCA.

Introduction

Star-shaped polymers are branched polymers that offer a wide range of possibilities for the design of new materials with unique properties.[1–3] The ability to control their architecture and the resulting properties opens up new avenues for their application in various fields, including drug delivery,[4–6] nanotechnology,[7–9] and materials science.[10–12] However, challenges remain, particularly in controlling the architecture of the star polymers and understanding the relationship between their structure and properties.[13–15]

Poly(ionic liquids) (PILs) are polyelectrolytes with ionic moieties incorporated into the repeating units. PILs are characterized by advanced applications in stimuli-responsive materials, biodegradable polymers, and catalytic processes.[16–18] One example of star-shaped poly(ionic liquids) (PILs) is based on polyhedral oligomeric silsesquioxane (POSS), a nanosized cage-like molecule that can be functionalized with various groups. By attaching PIL chains to the POSS core, star-shaped PILs with different ionic properties can be obtained, such as high ionic conductivity, low viscosity, and enhanced mechanical strength.[18] Another example is based on hyperbranched polystyrene (HBPS), a polymer with a highly branched structure and multiple terminal groups. By combining different polymerization techniques, a star-shaped PIL with HBPS core and imidazolium-based arms was prepared and used as an all-solid polymer electrolyte for lithium-ion batteries, showing good electrochemical performance and stability.[19] Star-shaped PILs with CD core and PIL chains with tunable host–guest interactions, such as reversible photoisomerization, thermo-responsive behavior, and selective recognition of guest molecules were also synthesized.[20–22]

This article presents the results of the synthesis and characterization of 8-arm star-shaped poly[2-(methacryloyloxy)ethyl trimethylammonium chloride]s (PMETA)s obtained by using (2-hydroxypropyl)-β-cyclodextrin (HP-β-CD) initiators in an enzymatically assisted ATRP, also known as breathing ATRP.

Results and discussion

In the literature, it is reported that the synthesis of linear PMETA was performed using aqueous solutions in both supplemental activators and reducing agents (SARA) and activators generated by electron transfer (AGET) ATRP methods. The SARA ATRP method showed a wide range of monomer conversions: with iron as the supplemental reducing agent (SRI), conversions were as high as 95%, while with copper, they ranged from 58% to 62%. Similarly, in experiments with ascorbic acid as SRI, conversions varied from 70% to 92%. For AGET ATRP, monomer conversion exceeded 90%. Both methods typically resulted in a dispersity index for PMETA of about 1.25 to 1.30.[23]

In our case star-shaped polymers were synthesized *via* enzymatically assisted ATRP method using β-CD derivatives as initiators with eight bromoester groups and thirteen hydroxyl groups, respectively (Fig. 1).[24] Moreover, the reaction was also carried out using HO-EBiB initiator, which yielded linear PMETA. Each reaction was carried out for 2 h at 45 °C. Star-

[a]*Department of Physical Chemistry and Technology of Polymers, Faculty of Chemistry, Silesian University of Technology, M. Strzody 9 Street, 44-100 Gliwice, Poland. E-mail: anna.mielanczyk@polsl.pl*

[b]*Department of Histology and Cell Pathology, School of Medicine with the Division of Dentistry in Zabrze, Medical University of Silesia, 41-808, Zabrze, Poland*

† Electronic supplementary information (ESI) available. See DOI: https://doi.org/10.1039/d5ra00674k

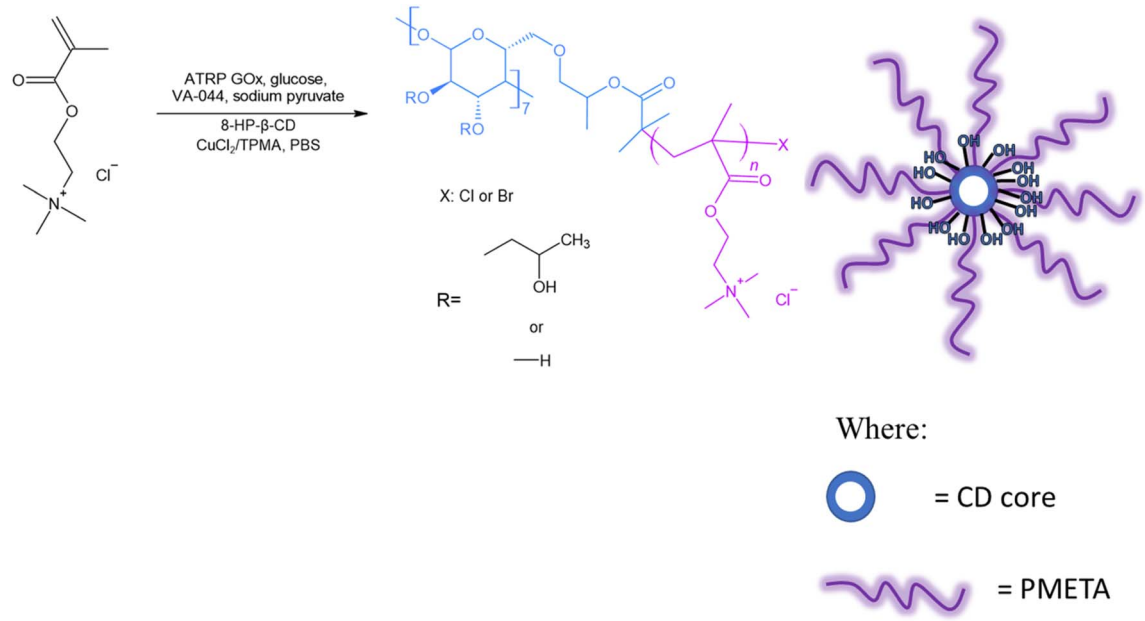

Fig. 1 Reaction scheme for the synthesis of star polymers.

shaped PMETAs (C1–C10) were obtained with 55–88% of monomer conversion. Reaction with HO-EBiB initiator, resulting linear PMETA (C0), proceeded with the monomer conversion equal 95%. Experimental procedures and characterization data are described in ESI.†

The ^{1}H NMR spectroscopy was used to confirm the successful synthesis and purification of the polymer, as well as to determine the META conversion, and theoretical molecular weight ($M_{n,NMR}$). The ^{1}H NMR spectra of the PMETAs showed characteristic signals for the META repeating units, and no signals for unreacted monomer (Fig. S1†). The molecular weight of C0 calculated from the analysis of the ^{1}H NMR spectrum is close to the value obtained from the SEC analysis. However, the dispersity is slightly higher than for the other polymers. Similar M_n values obtained from ^{1}H NMR and SEC analyses may be attributed to the negligible or minimal interaction between the tested polymers and the chromatographic column. In the case of star-shaped polymers, the significant discrepancies between the M_n values could suggest a stronger interaction with the chromatographic column. The molecular weight distribution of the polymers was in the range of obtained 1.06–1.12 which is proof that the polymers were synthesized in a high controlled manner (Fig. 2 and S2†).

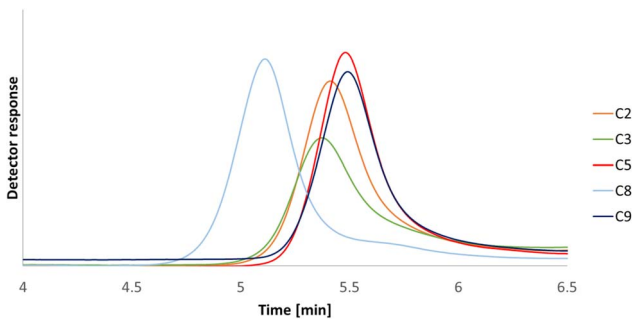

Fig. 2 SEC traces of eight-arm PMETA from RID detector.

The dispersity of 1.12 was obtained for the C3 polymer, and 1.06 for the C9 polymer. The addition of methanol caused better dissolution of the initiator in the reaction mixture, while increasing the conversion compared to reactions in which the initiator was added in the form of a solid. However, the dispersity of the polymers was not dependent on the method of introducing the initiator. At the same time, increasing the amount of methanol from 1.5 mL to 3 mL resulted in a decrease in conversion, which could be related to a decrease in enzyme activity, and thus the presence of oxygen in the reaction mixture. Changing the molar ratio of monomer to catalyst and changing the molar ratio of VA-044 in the case of C6 and C7 had no significant effect on dispersity and molecular weight. All polymers in this series were obtained with control over the reaction and were characterized by high homogeneity.

The thermal properties of PMETAs were studied by differential scanning calorimetry (DSC). As shown in Fig. S3† and Table 1, glass transition temperatures (T_g) corresponding to the PMETA arms were between 43.8 and 85.9 °C and stayed in good agreement with the literature.[25] Additional endothermal peaks were apparent at 209 (C2), 195 (C9), or 165 (C5) °C, corresponding to the HP-β-CD core melting point temperature (T_m).[24] All polymers underwent decomposition above 220 °C.

In the synthesis of PMETA *via* ATRP with methanol addition, there is a possibility that transesterification may lead to the formation of methyl methacrylate, and hydrolysis might result in choline acetate. These potential outcomes are suggested by signals in the ^{1}H NMR spectrum. Further, SEC curves indicating low molecular weight fractions could be indicative of these by-products. Such occurrences find parallels in similar cases

Table 1 Characteristics of obtained polymers[a]

Entry	$[META]_0 : [I]_0 : [VA\text{-}0440]_0 : [CuCl_2]_0 : [TPMA]_0$	Conversion [%]	DP	DP_{arm}	$M_{n,NMR}$ [g mol^{-1}]	$M_{n\ SEC,\ RID}$ [g mol^{-1}]	$Đ_{SEC,\ RID}$	T_g [°C]
C0	600 : 1 : 0.9 : 0.06 : 0.18	95%	570	—	118 400	125 000	1.33	62.2
C1	200 : 1 : 0.9 : 0.06 : 0.18	56%	112	14	23 300	2100	1.07	—
C2	200 : 1 : 0.9 : 0.06 : 0.18 (+1.5 mL MeOH with initiator)	88%	176	22	36 600	21 200	1.10	85.9
C3	200 : 1 : 0.9 : 0.06 : 0.18 (+3 mL MeOH with initiator)	78%	156	20	32 400	21 500	1.12	—
C4	400 : 1 : 0.9 : 0.06 : 0.18	73%	292	37	60 600	9200	1.11	—
C5	400 : 1 : 0.9 : 0.06 : 0.18 (+1.5 mL MeOH with initiator)	81%	324	41	67 300	18 500	1.09	43.8
C6	600 : 1 : 0.9 : 0.06 : 0.18	55%	330	41	68 500	3400	1.08	—
C7	600 : 1 : 1.2 : 0.06 : 0.18	63%	378	47	78 500	12 000	1.10	—
C8	600 : 1 : 0.9 : 0.06 : 0.18 (+1.5 mL MeOH with initiator)	64%	384	48	79 800	38 700	1.11	75.6
C9	800 : 1 : 0.9 : 0.06 : 0.18 (+1.5 mL MeOH with initiator)	65%	520	65	108 000	19 400	1.06	58.6
C10	450 : 1 : 0.9 : 0.06 : 0.18	56%	252	17	52 300	2800	1.08	—
C11	600 : 1 : 0.9 : 0.06 : 0.18	31%	186	12	93 000	2400	1.10	—

[a] Where: I – initiator for C0 was HO-EBiB and for C1–C11 was 8Br-HP-β-CD; $M_{n,NMR}$ – number average molecular weight based on ^{1}H NMR; $M_{n,RID}$ – number average molecular weight based on GPC, RID; $Đ$ – dispersity index based on GPC_{RID}; T_g – glass transition temperature from DSC scan.

reported in the literature, pointing to a consistent pattern in polymer synthesis involving ATRP and methanol.[26]

In order to describe the reaction kinetics, the polymerization reaction was performed under the same conditions as for the CP8 polymer. These measurements were performed by taking 0.2 mL samples before and after the reaction and every 20 minutes during the reaction (Fig. 3).

The examination of PMETA polymerization *via* ATRP kinetics, as evidenced by the provided data, reveals several critical characteristics indicative of a controlled polymerization process. Immediate initiation of the reaction is observed upon the addition of all reagents, as indicated by a 5% conversion at the outset, which occurs in the absence of external heating. This underscores the reactivity of the reagents or the exothermic nature of the reaction. A linear increase in monomer conversion from 5% to 54% over a 120-minute period suggests a consistent, controlled polymerization process, highlighted by the absence of abrupt spikes in conversion rate, thus indicating a stable reaction environment. The gradual, linear increase in conversion, along with the corresponding escalation in $M_{n,NMR}$ values (from 6600 g mol^{-1} to 67 600 g mol^{-1}), which represent the number-average molecular weight of the polymer, points to a controlled growth of the polymer chain. Such control is a characteristic feature of ATRP, where the polymerization is mediated through reversible deactivation of growing radical chains, resulting in a predictable and uniform increase in molecular weight without indications of uncontrolled reactions. The proportional increase in molecular weight with respect to polymerization time and conversion rate causes a narrow molecular weight distribution, a key attribute of controlled/living radical polymerizations. This level of control in the polymerization process is crucial for tailoring polymer properties for specific applications, enabling the synthesis of polymers with desired molecular weights and functionalities. Overall, the kinetics of ATRP, as delineated by the data, clearly demonstrate a controlled, predictable polymerization reaction, characterized by immediate initiation, linear progression of monomer conversion, and consistent molecular weight growth.

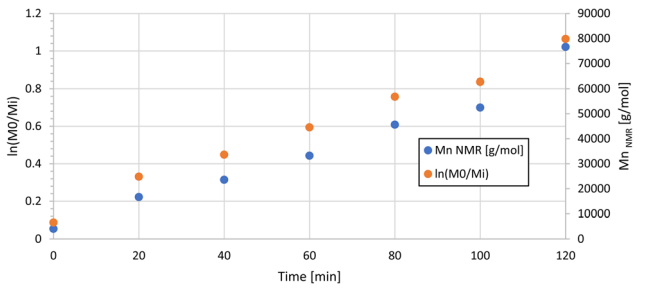

Fig. 3 A comparative graph showing monomer conversion (left ordinate, semi-logarithmic) and molecular weight change from NMR data (right ordinate) over polymerization time C8.

Experimental evaluations of water contact angles (WCA) and interfacial tension (IFT) were conducted utilizing glass plates, implementing both 5000 rpm and 1500 rpm and two concentrations of polymers' solutions 0.5 mg mL^{-1} and 5 mg mL^{-1} (Fig. 4 and S4–S10†).

In the experimental procedure, the spincoater's rotational velocity and the varying concentrations of the polymer solutions were chosen meticulously. This was done to ensure the fabrication of coatings with distinct thicknesses. It is hypothesized that these parameters play a pivotal role in influencing the final morphological characteristics of the deposited films. In the empirical investigation of the relationship between the spincoater's rotational speed and the contact angles of polymer coatings, a multifaceted correlation was observed. When the

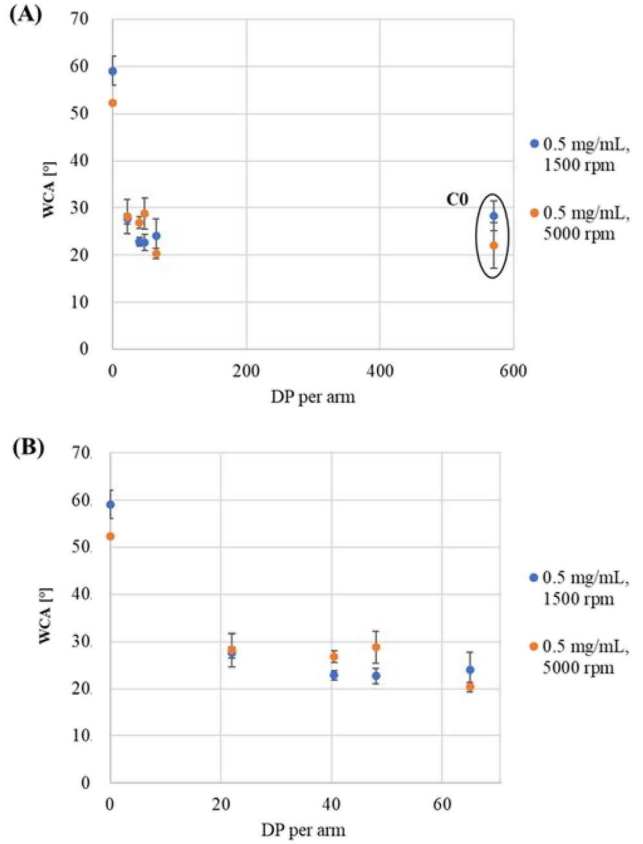

Fig. 4 WCA as a function of DP per arm of obtained polymers at a concentration of 0.5 mg mL^{-1} (A), a subset of the top graph showing only star-shaped polymers (B).

coatings were procured at a rotational speed of 5000 rpm, the contact angles displayed slightly diminished values in comparison to those produced at 1500 rpm. This observation was particularly pronounced in the case of coatings applied with polymer solutions at a concentration of 0.5 mg mL^{-1}. Further analysis revealed that the contact angle measured for polymeric coatings, except for the C4 polymer, decreased in a direct proportion to the increase in spin coater rotation speed for solutions at a concentration of 0.5 mg mL^{-1}. Conversely, in the case of polymer coatings from solutions with a concentration of 5 mg mL^{-1}, an inverse correlation between the speed of rotation and the contact angle values was noticeable in certain instances. However, a consistent pattern emerged when comparing the contact angle of polymer coatings applied with solutions at concentrations of 0.5 mg mL^{-1} and 5 mg mL^{-1}. In each case, at both rotational speeds, the polymer coatings from solutions with a lower concentration exhibited lower values of the water contact angle. By using a polymer concentration of 0.5 mg mL^{-1}, hydrophilic coatings were created with WCAs ranging from 20° to 29°, which are much lower than the WCA values for alkyd, epoxy, polyurethane or acrylic coatings.[27–29]

At elevated concentrations, discrepancies observed in the water contact angles can potentially be ascribed to the evolution of hydration shells around more intricate surface topographies. Such formation of hydration shells typically enhances the thermodynamic affinity between the aqueous phase and the polymer substrate. This implies that the molecular dynamics at the interface are profoundly influenced by the concentration-dependent morphological changes in the polymer, culminating in augmented water–polymer interactions. Consequently, these enhanced interactions can significantly dictate wettability properties and provide a mechanistic insight into the variations in contact angles at distinct concentrations.

The resulting data suggest a complex interplay between the rotational speed of the spincoater, the concentration of the polymer solution, and the contact angles of the coatings. For each of the examined coatings, a pronounced decrement in the contact angle was observed as a function of time. This temporal alteration in wettability properties can be attributed to the intrinsic solubility characteristics of the polymer in an aqueous environment (Fig. 5). At this point, it is fair to mention that the META is hygroscopic. Polymeric coatings prepared from PMETA may be influenced by environmental parameters such as humidity, temperature, and prolonged air exposure. Chemical modifications of the glass surface by PMETA *e.g. via* grafting reactions, could enhance coating robustness.

In the investigation of polymer coatings, particular emphasis was placed on the ITF parameter. Coatings deployed at a velocity of 5000 rpm (rpm) manifested specific behavioral patterns. For polymers' solution 5 mg mL^{-1}, excluding the C7 polymer, the IFT value for pure methanol was significantly higher compared to other tested polymers such as C2, C3, and C6, where the recorded values exhibited pronounced uniformity. The values for the remaining polymers were markedly lower. In the context of polymer coatings derived from solutions with a concentration of 0.5 mg, the IFT values at both examined velocities were inferior to the values for methanol alone. Furthermore, it was observed that the minimal values were typified by coatings with a linear polymer structure. A comparative analysis of the IFT values of the polymer coatings across both solution concentrations and both tested velocities revealed a consistent relationship for each of the examined polymers. Specifically, lower concentrations were characterized by reduced IFT values. This correlation lends further substantiation to the proposition that the obtained coatings are primarily characterized by their hydrophilic nature, a trait that was accurately detected by the implementation of stringent measurement protocols. Conversely, in the scenario of coatings applied at a reduced rotational speed of 1500 rpm for a concentration 5 mg mL^{-1}, the observed data did not delineate any visible trend in alignment with the value of pure methanol. This observation may be correlated with the intrinsic surface roughness of the applied coatings, a variable that is recognized to exert a considerable influence on the accuracy of IFT measurements. These insights indicate a multifaceted interaction between the rotational speed of the spin coater, the ensuing surface roughness, and the IFT values. More specifically, the roughness of the deposited coatings might be closely linked to the decreased rpm value of the spin coater, emphasizing the pivotal role of application techniques in defining the attributes of the resultant polymer films.

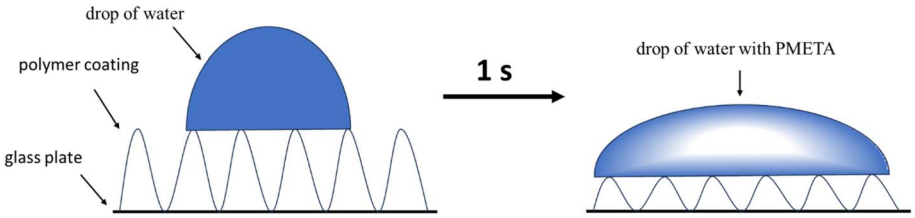

Fig. 5 Partial dissolution of PMETA at the point of contact between the coating and the water drop.

It was observed that the spincoater's rotational speed and the polymer solution's concentration significantly influenced the morphological characteristics of the coatings. This was evident in the variations of contact angles, with distinct differences noted between coatings produced at different rotational speeds and concentrations. The findings indicate that lower rotational speeds and higher concentrations result in increased surface roughness and hydration shell formation, which in turn affects the wettability properties of the coatings. It was found that at a higher rotational speed of 5000 rpm, the IFT values varied based on the polymer concentration and type, with notable differences in IFT values for different polymers at a 5 mg mL^{-1} concentration, and a consistent reduction in IFT values for lower concentrations. This suggests a strong correlation between the concentration of polymer solutions and the hydrophilic nature of the resultant coatings. The results indicate a clear dependency of these roughness parameters on both the polymer solution concentration and the spin-coating speed. Star-shaped polymers showed more pronounced surface irregularities under certain conditions compared to the linear polymer, highlighting the influence of molecular architecture on the coating's morphology.

IFT values for coatings prepared from star-shaped polymers at 1500 rpm and a concentration of 5 mg mL^{-1}, stayed in the range of 27–50 mN m^{-1}, which is typical for epoxy coatings.[30] Reducing the polymer concentration to 0.5 mg mL^{-1} and increasing the spin-coater speed to 5000 rpm results in IFT values comparable to those for acrylic coatings.[31]

The AFM data for star polymers C2, C5, C8, C9, and the linear polymer C0, when examined in the context of spin-coating, offers a profound insight into the nanostructured surfaces of polymer films (Fig. S11 and Table S1†). This detailed exploration is key to comprehending how the intrinsic polymer architecture and the conditions under which they are processed, particularly spin-coating speeds and solution concentrations, shape the resulting surface features at the microscopic level. The star polymers, with their varied monomer-to-initiator ratios, demonstrate significantly different surface roughness characteristics compared to the linear polymer C0.

Notably, the R_a and R_q values, representing the average and root mean square surface roughness, show a strong dependency on both the concentration of the polymer solution and the speed of spin-coating. At higher concentrations (5 mg mL^{-1}) and lower spin speeds (1500 rpm), the star polymers C2 and C5 exhibit higher R_a and R_q values, suggesting that increased polymer concentration results in more pronounced surface irregularities. The maximum vertical distance, Δz_{max}, further enhances our understanding of these surfaces by providing insight into the height variation across the polymer films. Star polymers, particularly under conditions of higher concentration and slower spin-coating speeds, display larger Δz_{max} values. This is indicative of a greater degree of topographical variation, likely a result of their more intricate molecular architecture when compared to linear polymers. Conversely, the linear polymer C0 shows a distinct surface characteristic profile. Under similar processing conditions, the roughness parameters of C0 are consistently lower than those observed in the star polymers. This is possibly due to the more uniform and less complex molecular structure of linear polymers, which leads to the formation of smoother coatings. An intriguing aspect of the data is the variation in coating thickness among the different polymers and under varying conditions. This suggests that the molecular structure of the polymers and the parameters used in spin-coating significantly impact the thickness of the final polymer film. This variation in thickness can have profound implications for the physical properties of the coatings, including their mechanical strength, optical clarity, and chemical resistance. In summary, the AFM study provides crucial insights into how molecular architecture and spin-coating conditions collectively influence the nanoscale morphology of polymer films. This knowledge is essential in fields where surface properties play a pivotal role in the performance of the material, such as in coating technologies, biomedical device fabrication, and various nanotechnology applications. This data lays a solid foundation for future research aimed at optimizing polymer coatings for specific applications, ensuring tailored functionality and performance. Understanding these relationships is fundamental for advancing materials science, particularly in the area of polymer chemistry and surface engineering, where precise control over nanostructures can lead to enhanced material properties and novel applications.

Conclusions

In this work, star-shaped polymers with META arms and cyclodextrin-based core were synthesized by enzymatically assisted ATRP in the presence of air. The polymers were characterized by ^{1}H NMR, and GPC analyses. The well-defined star-polymers obtained using as well as solution of initiator in methanol as a solid initiator were characterized by very tight molecular distributions (M_w/M_n < 1.12). This work provides

a novel strategy to synthesize well-defined star-shaped polymers in accordance with the principles of green chemistry. The study also explored the hydrophilic nature of polymer coatings compared to methanol-treated plates, with factors such as rotational speed and concentration influencing WCA values. IFT exhibited specific behavioral trends, with the values for most polymers being noticeably lower than pure methanol, except at reduced speeds where the data became inconsistent. These findings underline a complex interplay between the spin coater's rotational speed, surface roughness, and IFT values, highlighting the critical role of application methods in defining the characteristics of the resultant polymer films.

The polymers obtained in this study exhibit high solubility in aqueous media, a characteristic that poses challenges for their utilization as coatings. To adapt these polymers for coating applications, chemical modifications are imperative to attenuate their solubility in water. Strategies such as cross-linking or the incorporation of hydrophobic moieties could be employed to achieve this objective.

Conversely, these polymers' inherent hydrophilic nature and expansive spatial configuration render them promising candidates for other applications. Specifically, their structure and properties are conducive to controlled drug release systems. The hydrophilic domains can facilitate the encapsulation of therapeutic agents, while the spatial structure can modulate the release kinetics. Moreover, these polymers could be advantageous in environmental engineering applications, particularly in the adsorptive removal of contaminants from aqueous systems. The unique topology and three-dimensional structure of these polymers could engage in interactions with pollutants, thereby facilitating their removal from aqueous environments. The intricate spatial arrangement provides multiple sites for adsorption and complexation with contaminant molecules, enhancing the efficiency of pollutant removal.

Data availability

The data supporting this article have been included within the article and as part of the ESI.†

Conflicts of interest

The authors declare no competing interests.

Acknowledgements

This research was funded by the Polish Budget Funds for Scientific Research in 2023 and 2024 as core funding for R&D activities at the Silesian University of Technology-funding for young scientists, grant number BKM-545/RCH4/2023 (04/040/BKM23/0259), BKM-538/RCH4/2024 (04/040/BKM24/0287), 1st degree pro-quality Silesian University of Technology Rector's grant number 04/040/RGJ24/0274 and the grant for starting research on a new subject no. 32/014/SDU/10-22-68 of the Rector of Silesian University of Technology.

References

1 J. H. Vrijsen, C. Osiro Medeiros, J. Gruber and T. Junkers, *Polym. Chem.*, 2019, **10**, 1591–1598.
2 S. Ludwanowski, O. Skarsetz, G. Creusen, D. Hoenders, P. Straub and A. Walther, *Angew. Chem., Int. Ed.*, 2021, **60**, 4358–4367.
3 A. Mielańczyk, M. Kupczak, O. Klymenko, Ł. Mielańczyk, S. Arabasz, K. Madej and D. Neugebauer, *Polym. Chem.*, 2022, **13**, 4763–4775.
4 D. Srivastva and A. Nikoubashman, *Polymers*, 2018, **10**(6), 599.
5 J. Liu, H. Duong, M. R. Whittaker, T. P. Davis and C. Boyer, *Macromol. Rapid Commun.*, 2012, **33**, 760–766.
6 G. M. Soliman, R. Sharma, A. O. Choi, S. K. Varshney, F. M. Winnik, A. K. Kakkar and D. Maysinger, *Biomaterials*, 2010, **31**, 8382–8392.
7 A. Fus-Kujawa, P. Teper, M. Botor, K. Klarzyńska, Ł. Sieroń, B. Verbelen, M. Smet, A. L. Sieroń, B. Mendrek and A. Kowalczuk, *Int. J. Polym. Mater. Polym. Biomater.*, 2021, **70**, 356–370.
8 D. J. Cameron and M. P. Shaver, *Chem. Soc. Rev.*, 2011, **40**, 1761–1776.
9 H. Forgham, J. Zhu, R. Qiao and T. P. Davis, *ACS Appl. Polym. Mater.*, 2022, **4**, 6784–6796.
10 I. Bos, P. Van der Scheer, W. G. Ellenbroek and J. Sprakel, *Soft Matter*, 2019, **15**, 615–622.
11 W. H. Binder and R. Sachsenhofer, *Macromol. Rapid Commun.*, 2008, **29**, 952–981.
12 M. Liu, J. R. Blankenship, A. E. Levi, Q. Fu, Z. M. Hudson and C. M. Bates, *Chem. Mater.*, 2022, **34**, 6188–6209.
13 A. Skandalis, T. Sentoukas, D. Giaouzi, M. Kafetzi and S. Pispas, *Polymers*, 2021, **13**, 1698.
14 Y. Masubuchi, G. Ianniruberto and G. Marrucci, *Nihon Reoroji Gakkaishi*, 2021, **49**, 171–178.
15 P. Polanowski, K. Hałagan and A. Sikorski, *Polymers*, 2022, **14**, 2522.
16 D. Neugebauer, A. Mielańczyk, R. Bielas, J. Odrobińska, M. Kupczak and K. Niesyto, *Pharmaceutics*, 2019, **11**, 337.
17 H. Mori, Y. Ebina, R. Kambara and K. Nakabayashi, *Polym. J.*, 2012, **44**, 550–560.
18 Z. He, M. Zhong, Y. Yang, C. Wu and J. Yang, *J. Polym. Res.*, 2016, **23**, 3–7.
19 A. Wang, H. Xu, X. Liu, R. Gao, S. Wang, Q. Zhou, J. Chen, X. Liu and L. Zhang, *Polym. Chem.*, 2017, **8**, 3177–3185.
20 W. Yu, L. Liu, F. Li and Z. Tan, *J. Ind. Eng. Chem.*, 2021, **103**, 322–328.
21 A. Bouyahya, B. S. Sembo-Backonly, A. Favrelle-Huret, S. Balieu, F. Guillen, V. Mesnage, C. Karakasyan-Dia, M. Lahcini, D. Le Cerf and G. Gouhier, *Environ. Sci. Pollut. Res.*, 2022, **29**, 271–283.
22 S. Y. Zhang, Q. Zhuang, M. Zhang, H. Wang, Z. Gao, J. K. Sun and J. Yuan, *Chem. Soc. Rev.*, 2020, **49**, 1726–1755.
23 C. Visnevskij and R. Makuska, *Macromolecules*, 2013, **46**, 4764–4771.
24 T. Fronczyk, A. Mielańczyk, O. Klymenko, K. Erfurt and D. Neugebauer, *Molecules*, 2023, **29**, 55.

25 M. Isik, R. Gracia, L. C. Kollnus, L. C. Tomé, I. M. Marrucho and D. Mecerreyes, *ACS Macro Lett.*, 2013, **2**, 975–979.
26 Y. Li, S. P. Armes, X. Jin and S. Zhu, *Macromolecules*, 2003, **36**, 8268–8275.
27 I. H Ifijen, N. U Udokpoh, G. E Onaiwu, E. M Jonathan and E. U Ikhuoria, *Momona Ethiop. J. Sci.*, 2022, **14**, 1–31.
28 S. Ji, H. Gui, G. Guan, M. Zhou, Q. Guo and M. Y. J. Tan, *Prog. Org. Coat.*, 2021, **153**, 106140.
29 H. J. Perera, B. K. Khatiwada, A. Paul, H. Mortazavian and F. D. Blum, *J. Appl. Polym. Sci.*, 2016, **133**(41), 44072.
30 J. R. Abbott and B. G. Higgins, *J. Polym. Sci., Part A:Polym. Chem.*, 1988, **26**, 1985–1988.
31 K. Grundke, S. Michel and M. Osterhold, *Prog. Org. Coat.*, 2000, **39**, 101–106.